

**PCCP****Plasmonic Sphere-On-Plane Systems with Semiconducting Polymer Spacer Layers**

Journal:	<i>Physical Chemistry Chemical Physics</i>
Manuscript ID	CP-ART-02-2018-001314.R1
Article Type:	Paper
Date Submitted by the Author:	20-Mar-2018
Complete List of Authors:	Yu, Binxing; Rutgers University, Chemistry & Chemical Biology Tracey, Jill; Rutgers University, Chemistry & Chemical Biology Cheng, Zhongkai; Rutgers University, Chemistry and Chemical Biology Vacha, Martin ; Tokyo Institute of Technology O'Carroll, Deirdre; Rutgers University, Materials Science and Engineering; Rutgers University, Chemistry and Chemical Biology

SCHOLARONE™
Manuscripts

Plasmonic Sphere-On-Plane Systems with Semiconducting Polymer Spacer Layers

Binxing Yu¹, Jill I. Tracey¹, Zhongkai Cheng¹, Martin Vacha², and Deirdre M. O'Carroll^{1,3}*

¹ Rutgers University, Department of Chemistry & Chemical Biology, 610 Taylor Road, Piscataway, NJ 08854, USA

² Tokyo Institute of Technology, Department of Materials Science & Engineering, Ookayama 2-12-1, Meguro-ku, Tokyo, Japan

³ Rutgers University, Department of Materials Science and Engineering, 607 Taylor Road, Piscataway, NJ 08854, USA

*Corresponding Author. E-mail: ocarroll@rutgers.edu

Keywords: scattering; plasmonic coupling; nanoparticles; conjugated polymers; sphere-on-plane

Abstract

The optical properties of metal-film-coupled nanoparticles (NPs) are highly sensitive to physical and optical interactions between the NPs and the spacer medium in the gap between the NP and metal film. Here, we investigate the physical and optical interactions between gold NPs (AuNPs) and semiconducting conjugated polymer thin-film spacers in a “sphere-on-plane” type metal-film-coupled NP system, and their influence on the plasmonic scattering of individual AuNPs. We choose two different conjugated polymers: one with an absorption spectrum that is resonant with the plasmonic modes of the AuNPs and another that is non-resonant. By correlating dark-field back-scattering optical images with topographic atomic force microscope images, we find that partial embedding of the AuNPs occurs in both conjugated polymers to different extents. This can lead to partial quenching of certain plasmonic scattering modes, which results in a change of the back-scattering colors from the AuNPs. Pronounced, red-shifted scattering is observed due to deep embedding of the AuNPs, particularly for thicker conjugated polymer spacers that have resonant absorption with the plasmonic modes of the AuNPs. Polarization-controlled defocused dark-field imaging is employed to visualize the emergence of horizontally-polarized scattering modes upon embedding of AuNPs into the conjugated polymer spacer. These results demonstrate the importance of nanoparticle-spacer physical interactions to the control of the color and polarization of coupled plasmonic modes in nanoparticle-film systems relevant to surface plasmon-based optical devices.

Introduction

Metal-film-coupled plasmonic nanoparticles (NPs), i.e., “sphere-on-plane” (SOP) systems, have emerged as platforms for many plasmon-mediated optical enhancement applications and have prompted numerous studies to understand and manipulate the electromagnetic modes in these systems [1-23]. In such SOP systems, the metal film not only supports image charges induced by the NP, but it can also support propagating surface plasmon polariton (SPP) modes, which can couple with the excited localized surface plasmon resonance (LSPR) modes of the NP and give rise to plasmonic gap modes [2,3]. As a result, the nanogaps between NPs and metal films behave like hot spots with extremely-intense, localized electric field concentration at visible frequencies that can be used for enhanced nanoscale signal detection [4,5]. In the late 1980s, Wind et al. [4,7] and Ruppin [8] introduced an analytical model using quasistatic image charge theory for a SOP system. Later plasmon hybridization models provided deep physical insights into the coupled plasmonic modes [9,10]. Then, Smith and co-workers identified coupling modes arising from interactions between LSPRs and SPPs in SOP systems [11,12], and Kik and co-workers demonstrated the observation of image dipole coupling modes for metal-film-coupled plasmonic nanoparticles [13,14].

Recently, we demonstrated control of plasmonic coupling modes in a SOP system that consists of a 10 nm- to 50 nm-thick absorptive, semiconducting polymer spacer layer sandwiched between a metal NP and a metal film [23]. This particular SOP system

provides a platform to manipulate light trapping in the absorptive spacer layer, as evident from the spectral dependence of scattering on the thickness of the spacer layer, the metal film and the shape and size of the NPs. However, thus far, most previous investigations have been focused primarily on the SOP systems consisting of single NPs and metal films separated by a transparent medium, e.g. Al_2O_3 or polyvinylalcohol (PVA) layers between 0 nm and 5 nm in thickness [2,3]. The physical interactions between plasmonic NPs and absorptive conjugated (i.e., semiconducting) polymer spacers have not been experimentally investigated. As a result, little is known about the influence of absorptive spacers on the optical/plasmonic modes present, as well as their effects on the spectral response of NPs in an SOP system.

In this work, we employ resonant and non-resonant semiconducting conjugated polymer spacers in SOP systems consisting of AuNPs and underlying Au thin films. The influence of the spacer's physical and optical characteristics on the light scattering behavior of individual AuNPs is studied. Our results show that partial embedding of AuNPs into a poly(3-hexylthiophene) (P3HT) resonant absorptive spacer can lead to damping or absorption of the plasmonic coupling modes, which further results in a range of back-scattering colors from AuNPs under dark-field (DF) illumination. However, the back-scattering colors are not substantially changed when a non-resonant, poly(9,9-dioctylfluorene) (PFO) spacer is employed that only absorbs light with wavelengths shorter than the wavelengths at which the plasmonic modes of the SOP

system occur, despite partial embedding of the NP. Moreover, dark-field spectroscopy and electromagnetic simulations reveal that the plasmonic coupling between horizontally-polarized LSPRs supported by the AuNPs and SPPs supported by the metal film is enhanced with deeper embedding. Finally, polarization-controlled, defocused DF imaging is employed to visualize the emergence of more dominant horizontally-polarized modes upon embedding of AuNPs into the P3HT thin film. These results demonstrate the importance of NP-spacer physical and optical interactions for tuning plasmonic coupling modes in SOP systems.

Results and Discussion

Figure 1 a,b shows schematics of the two types of SOP systems studied here. The first type is the AuNP/P3HT/Au film SOP system and the second type is the AuNP/PFO/Au film SOP system. In the fabricated samples (see Experimental Section), the AuNPs had a diameter of $101.5 \text{ nm} \pm 15.1 \text{ nm}$ (nominally 100 nm) and the Au films had a thickness of 35 nm in all cases. The P3HT and PFO thin films had two thicknesses, 20 nm and 50 nm, in order to study how the distance between the AuNP and the underlying Au film affects the plasmonic response of the SOP system. P3HT was chosen because its optical absorption spectrum overlaps with the localized surface plasmon resonance (LSPR) mode of the AuNPs (Figure 1c); hence, its absorption is “resonant” with the AuNP. In contrast, PFO was chosen as a conjugated polymer spacer for

comparison with the P3HT spacer due to the short-wavelength absorption band of PFO (i.e., high bandgap) which does not spectrally overlap with the LSPR or plasmonic coupling modes of the SOP system (which occur at wavelengths longer than 500 nm); see Figure 1c. Therefore, PFO's absorption can be said to be non-resonant with the AuNP and, therefore, was not expected to optically absorb localized electromagnetic fields associated with the plasmonic modes of the SOP system.

The ensemble-averaged DF back-scattered light enhancement spectra of AuNP/P3HT/Au film and AuNP/PFO/Au film SOP systems are shown in Figure 2a, relative to the corresponding conjugated polymer/Au film without AuNPs (see Experimental Section), for samples with polymer film thicknesses of 20 ± 2 nm (nominally 20 nm). The DF spectrum of a AuNP on glass is also shown for comparison. It is evident that the dominant scattering peak from the AuNP/PFO/Au film sample was similar in wavelength to that of the AuNP on glass, apart from a slight shoulder at longer wavelengths and a dip at shorter wavelengths. In contrast, the main scattering peak from the AuNP/P3HT/Au film sample was blue-shifted compared to the AuNP on glass and a new, well-defined peak at a wavelength of ~ 660 nm emerged.

Under DF optical illumination, individual AuNPs of similar size exhibited similar back-scattered light intensities in the AuNP/P3HT/Au film SOP system, but had distinct scattering color variations; examples of "red" and "green" AuNPs are shown in Figure 2c. The color variations suggested that there were differences in the local environment of individual particles and/or differences in the electromagnetic interaction between the

AuNPs and the substrate [13,23]. Corresponding scanning electron microscopy (SEM) images of the AuNPs in the same sample area (see Figure 2b insets) showed that there was not a significant size difference between the “red” AuNP and “green” AuNP - an observation that was consistent throughout all SOP samples. However, variations in the roughness of the P3HT film were apparent in the SEM image. This suggested that the color variations in the DF back-scattering from AuNPs in the AuNP/P3HT/Au film SOP system could be attributed to variations in physical interactions between AuNPs and the underlying P3HT film, which concomitantly affect electromagnetic interactions between the AuNPs and the underlying P3HT/Au film. This also indicates that the two peaks observed in the ensemble-averaged DF back-scattering spectrum of the AuNP/P3HT/Au film system in Figure 2a arose from two distinct populations of AuNPs with different scattering colors. In contrast, DF optical images of the AuNP/PFO/Au film systems did not exhibit notable color changes across a particular SOP sample.

To further investigate the physical and electromagnetic properties of the SOP system, correlated AFM topography and DF back-scattered light images of AuNPs on the different spacer layers were acquired. AFM and DF images of AuNPs on glass substrates were also acquired for comparison. In order to correlate the heights of individual AuNPs measured by AFM with nanoparticle scattering color, first, regions of different samples were labeled in DF optical images and, subsequently, the same regions were then imaged using AFM. Figure 3a-e shows the AFM topography images and corresponding DF back-scattered light images of AuNPs on P3HT and PFO spacer films (with thicknesses

of 20 nm and 50 nm, in each case) on 35 nm-thick Au films, and, of AuNPs directly on a glass substrate. Histograms of AuNP heights are shown in Figure 3f and the heights were extracted from AFM topography images taken of several random areas of each sample type. In total, the height of more than 50 AuNPs from each sample type were analyzed (Supporting Information, Figure S1). The DF optical images revealed that a certain fraction of AuNPs exhibited red/orange scattering colors on both 20 nm- and 50 nm-thick P3HT spacers. It was apparent that, typically, the AuNPs on P3HT that exhibited red scattering were also the AuNPs that had the smallest heights.

In the histogram of AuNP heights, it can be seen that, compared to AuNPs on glass (mean height of $111.3 \text{ nm} \pm 8.8 \text{ nm}$), the mean height of the AuNPs was reduced on both P3HT and PFO. Since the AuNPs on glass came from the same AuNP dispersion as those on both P3HT and PFO, the lower height of AuNPs on the conjugated polymers indicated that the AuNPs were partially embedded in both the P3HT and PFO spacers (the mean height of the AuNPs on the different conjugated polymer spacers ranged from 91 nm to 96 nm). Furthermore, on PFO, AuNP heights were slightly greater, on average, than those on P3HT and it was also apparent that the extent of AuNP embedding was slightly greater on the thinner conjugated polymer spacers (the mean height of the AuNPs was $93.4 \text{ nm} \pm 12.7 \text{ nm}$ and $91.9 \text{ nm} \pm 13.3 \text{ nm}$ on 20-nm-thick PFO and P3HT, respectively, and $96.0 \text{ nm} \pm 10.3 \text{ nm}$ and $95.1 \text{ nm} \pm 13.1 \text{ nm}$ on 50-nm-thick PFO and P3HT, respectively).

One possible physical interaction between AuNPs and the conjugated polymer spacer that could explain the observed trends in partial embedding of the AuNPs is the local deformation of the spacer in response to the pressure induced by the mass of the AuNP. For example, the elastic (Young's) moduli of PFO and P3HT thin films range between 0.25 and 20 GPa [24-30], which are more than an order of magnitude less than that of glass. In particular, on P3HT, a fraction of the AuNPs exhibited heights less than 80 nm, which were significantly smaller than the peak value of the height distribution at ~95 nm. In other words, it is likely that a small fraction of the AuNPs were partially embedded into the P3HT spacer to a relatively significant extent, i.e., up to ~30 nm in some cases. By comparing the heights of the AuNPs and their scattering color, it was apparent that the range of scattering colors shown from red to green corresponded to AuNP heights from low to high in 2D AFM height profiles (Figure 3a,c) and, therefore, to different extents of embedding. Additionally, it was revealed by AFM analysis that the root-mean-square (RMS) roughness of the P3HT surface was ~1.5 nm, which can potentially lead to significant variation in the contact area between a given AuNP and the underlying conjugated polymer thin-film spacer, and, hence, significant spectral variation in their scattering response [31]. Therefore, the variations in embedding and back-scattering color observed for AuNPs on P3HT may be attributed to the collective effects of the relative softness of P3HT thin films, their surface roughness and the mass of 100 nm-diameter AuNPs. Additional effects may also be at play such as: possible electrostatic attraction between electrons accumulated at the surface of PVP-coated

AuNP (surface zeta potential is -29 mV [32]) and the holes in P3HT; and enhancements in the red fluorescence from P3HT for AuNPs that are more deeply embedded.

For PFO, despite the lack of deeply-embedded AuNPs, a distribution of heights of AuNPs was also observed (attributed to partial embedding; Figure 3b,d,f); however, no corresponding color variation was apparent in the DF optical images (Figure 3b,d) - the back-scattered color of AuNPs on a PFO spacer was predominantly green. Since PFO has an absorption band below ~ 410 nm (Figure 1c), plasmonic modes of the SOP system are not expected to be absorbed by PFO even when the AuNP is partially embedded. A uniform blue background, arising from the strong blue fluorescence of the PFO film, was also apparent in the DF images (Figure 3b,d); particularly for the thicker (50 nm) PFO film. The PFO optical properties together with the relatively smooth PFO surface (RMS roughness < 0.5 nm) could account for the prevailing green color of AuNPs on PFO observed in the DF optical images (Figure 3a-e). Therefore, the presence of back-scattering color variations for AuNPs on P3HT spacers but the lack of such variations with PFO spacers, was attributed to the difference in optical absorption band wavelengths between P3HT and PFO in addition to partial-embedding of the AuNPs into the conjugated polymer spacer, and the resulting difference in the degree of spectral and spatial overlap with the plasmonic modes of the SOP system.

Since the scattering from AuNPs and the refractive index of the P3HT or PFO spacers can work synergistically to overcome the wavevector mismatch between incident

light waves and SPPs supported by the metal film, it was expected that both LSPRs and SPPs were present in the SOP system under study. In our earlier study, we proposed four plasmonic coupling modes in an AuNP/P3HT/Au SOP system: horizontal image dipole coupling (L_1), vertical image dipole coupling (L_2), horizontal LSPR-SPP coupling (L_3) and vertical LSPR-SPP coupling (L_4) [23]. For a thick (~ 50 nm) spacer, image dipole coupling (L_1 and L_2) becomes very weak due to the exponential decay of the LSPR local electric field intensity [33], and, thus, for larger film thicknesses, LSPR-SPP coupling (L_3 , L_4) dominates over image dipole coupling and occurs at wavelengths red-shifted from the LSPR wavelength. This is due to the fact that SPP modes can not only propagate relatively easily on Au films at longer wavelengths, but their local electric field intensities can decay over a distance greater than 100 nm in the vertical direction (i.e., normal to the plane of metal film) [34].

Figure 4 shows back-scattered light spectra, computed using three-dimensional (3D) finite-difference-time-domain electromagnetic simulations, for the SOP systems under study here, both with and without AuNP embedding. The SOP systems were excited with a broadband, total-field scattered-field source and that enabled broadband illumination and collection of the back-scattered light spectrum. The source was incident $\sim 10^\circ$ with respect to the surface normal; therefore, it was predominantly in-plane (i.e., horizontally) polarized but had a slight out-of-plane (i.e., vertically) polarized component to enable excitation of both in-plane- and out-of-plane- polarized plasmonic modes of the system.

For the AuNP/P3HT/Au film SOP system, partial embedding of the AuNP in the P3HT spacer resulted in increased scattering at orange/red wavelengths (> 600 nm) attributed to a horizontally-polarized L_3 mode, and a reduction in the scattering peaks at green-yellow wavelengths (~ 550 nm) attributed to L_1 (Figure 4b,d) [23]. With more of the AuNP embedded in the P3HT spacer, the vertical LSPR is expected to couple to the in-plane SPP mode more strongly, which results in poor radiation into the far field and further leads to the inefficient out-coupling of L_4 as scattered light [23]. This indicates that with AuNPs embedded into the spacer, the coupling mode at longer wavelength was horizontally-polarized in nature.

Interestingly, the simulated back-scattered spectrum for the AuNP/PFO/Au film SOP system exhibited similar shape to that with a P3HT spacer for spacer thicknesses of 20 nm (Figure 4a,b). Without AuNP embedding, the scattering wavelength occurred predominantly in the 550 nm to 600 nm wavelength range for both cases; corresponding to a yellow color. The scattering intensity was slightly weaker for the P3HT case due to the resonant absorption of the P3HT. However, since the polymer thin films were optically thin, the majority of the light was back-scattered rather than absorbed by the polymer. With 15 nm of AuNP embedding in the polymer film, the back scattering spectra were reduced in intensity and the dominant peak (attributed to the L_3 mode) occurred in the 640 nm to 670 nm wavelength range. Weak scattering in the 500 nm to 550 nm wavelength range was also apparent. Given the similarities between the

back-scattered light spectra for SOP systems with 20 nm-thick PFO and P3HT spacers, the optical properties of the spacer did not appear to play a significant role in the scattering color changes in that case. Instead, the nanoparticle embedding was responsible for significant changes in the back-scattered light spectra. In contrast, when the spacer thickness was increased to 50 nm, clear differences emerged between the simulated back-scattering spectra of the SOP systems with P3HT and PFO (Figure 4c,d). For PFO, the back scattering spectra were similar with and without embedding, with prevalent scattering in the yellow-orange wavelength range (550 nm to 620 nm) and a slight red shift for the embedded case. For P3HT, the AuNP LSPR mode (L_1) at ~550 nm was strongly absorbed. Therefore, clearly, for thicker spacers, the absorption wavelength of the spacer played a greater role in changing the back-scattering color of embedded AuNPs.

In the experimentally-measured DF spectra and images (Figure 2a and Figure 3), given the apparent lack of red back-scattering for AuNPs on both 20 nm- and 50 nm-thick PFO spacers compared to AuNPs on P3HT spacers, it is likely that the extent of physical interaction between the AuNPs and the PFO spacers was not very significant - both because of less embedding and because of smoother PFO thin films compared to the corresponding P3HT case. In the simulated spectra, for the thicker spacer (50 nm), as the extent of embedding increased, the scattering in the green-yellow wavelength range remained high for the PFO spacer but decreased for the P3HT spacer (Figure 4c,d). This

was consistent with the experimental results of Figure 3 and with the high absorption coefficient of P3HT at green wavelengths where the L_1 plasmonic mode resides (Figure 1c). Therefore, it was concluded that L_1 was primarily absorbed by the thicker P3HT spacer as embedding increased, leading to the observation of prominent scattering at red wavelengths (from the horizontal LSPR-SPP coupling mode, L_3). In contrast, L_1 was not absorbed by the 50 nm PFO spacer; hence the prevalence of green-yellow scattering.

For the aforementioned plasmonic coupling modes, the previous results confirm that partial embedding can alter their relative strengths and, hence, the back-scattering colors of individual AuNP/P3HT/Au film SOP systems. Furthermore, our prior theoretical work along with the simulated data in Figure 4 indicates that the polarization of the back-scattering from the SOP systems should be altered by AuNP embedding in the polymer film. To experimentally verify the effect of partial embedding on the polarization direction of the plasmonic coupling, we employed defocused DF imaging, which has the capability of determining the three-dimensional (3D) orientation of single molecule/particle without angular degeneracy. However, since polarization-based imaging methods are not achievable with traditional white light illumination and laser-excited imaging methods cannot ensure the excitation of all plasmonic coupling modes at the same time, a pseudo-DF imaging method with a broadband laser source was employed. A supercontinuum laser with coherent illumination spanning wavelengths of 400 nm to 2400 nm was used for excitation. The incident angle was set to 88° in order to

create near-grazing-incidence, polarized illumination (Figure 5a). The out-of-plane polarization angle, Ψ , of the scattering from AuNP/polymer spacer/Au film samples was determined by comparing single-AuNP defocused DF images (Figure 5b) and defocused photoluminescence (PL) images of single molecules reported in the literature [35,36], with $\Psi = 90^\circ$ corresponding to a completely vertical polarization (i.e., parallel to the Z-axis) and 0° corresponding to a horizontal polarization (i.e., in the X-Y plane); see Figure 5a.

The defocused DF images were analyzed using radial line profiles and compared with the literature defocused PL profiles [37,38]. AuNPs with scattering modes polarized vertically showed a ring-shaped scattering pattern in the defocused DF image, while AuNPs with more in-plane (i.e., horizontally) polarized scattering appeared more anisotropic or distorted in the defocused DF image. Representative single-nanoparticle defocused DF images from AuNP/polymer spacer/Au film samples are shown in Figure 5b along with the approximated Ψ angle. Figure 5c shows histograms of the out-of-plane polarization angle, Ψ , for single AuNPs in SOP systems with various polymer spacer materials and thicknesses under p-polarized illumination. When a 20 nm-thick PFO film was used as the spacer layer, most of the AuNPs exhibited vertically-polarized scattering under p-polarized excitation. However, more horizontally-polarized components were observed with a thicker spacer. This was probably due to the fact that, with a thinner spacer, the coupling between an AuNP dipole and its image dipole in the underlying

metal film is stronger in the vertically-polarized direction (Z -direction). In contrast, the direction of a horizontally-polarized NP dipole and that of its image dipole are expected to be antiparallel, resulting in a weaker net dipole moment. Accordingly, this led to much stronger vertically-polarized scattering which was easily excited under p-polarized illumination.

With a thicker spacer, the coupling between the AuNP particle dipole and its image dipole was weakened, which resulted in weaker vertically-polarized scattering. As a result, the vertically-polarized component of the scattering dropped compared with that for the thinner spacer case. With regard to P3HT spacers, at a thickness of 20 nm, the polarization of the scattering was still primarily vertical which was similar to PFO (Figure 5c). However, when the P3HT spacer thickness was increased to 50 nm, not only did the vertically-polarized component decrease, but also the horizontally-polarized component became dominant, which was not observed in the 50 nm-thick PFO case. This behavior was attributed to the partial embedding of AuNPs into the P3HT spacer. As indicated from the simulated back-scattering spectra (Figure 4), for a 50-nm-thick P3HT spacer, with an AuNP partially embedded in the spacer, the LSPR-SPP coupling mode, L_3 , which is a horizontally-polarized mode in nature, becomes predominant. This agrees with the observation that more AuNPs embedded into the P3HT spacer resulted in more horizontally-polarized scattering components in the defocused DF images. In addition, with embedding, the optical transition dipole moment of the polymer could interfere with

the plasmonic coupling modes of the SOP system, which would result in more complex scattering behavior [21,5].

Conclusions

For a AuNP/conjugated polymer/Au film sphere-on-plane system, partial embedding of AuNPs into the conjugated polymer thin film was confirmed by atomic force microscopy and the effects of partial embedding on the plasmonic gap modes and on the back-scattering color of individual AuNPs were investigated. We found that the partial embedding was largely dependent on the mechanical properties and the thickness of the conjugated polymer spacer. Furthermore, the back scattering color was altered upon AuNP embedding. For thin conjugated polymer spacers (20 nm) the extent of embedding played a more significant role in changing the back-scattering color than the optical properties of the spacer. For thicker spacers (50 nm), both the extent of embedding and the degree of spectral overlap between the polymer's absorption band and the plasmonic modes of the system played significant roles in determining the back-scattering color. Polarization-resolved defocused dark-field imaging also proved the more enhanced horizontally-polarized nature of the plasmonic scattering upon deeper embedding. We believe this study connects the optical response and physical interaction in an SOP system and offers new insights for enhancing and spectrally tuning light in ultra-thin film based optoelectronics.

Experimental Section

Sample Fabrication: To fabricate the desired SOP system, a thin film of Au was deposited onto a pre-cleaned glass substrate by thermal evaporation to a thickness of 35 nm, as measured by a quartz crystal monitor. The resulting thickness was also confirmed using atomic force microscopy (AFM). Subsequently, the conjugated polymer (either P3HT (American Dye Source, Inc) or poly(9,9-dioctylfluorene) (PFO) (Sigma-Aldrich)) in chloroform solvent was heated to 45 °C, stirred for 15 min., sonicated for another 20 min., filtered (using a 0.2 µm pore size filter) and then spin-coated onto the Au thin film. The concentration of the conjugated polymer solution was varied between 2 mg/mL and 10 mg/mL to control the thickness of conjugated polymer spacer to between 20 nm and 50 nm, as measured by AFM. After drying the samples in a desiccator for 20 min., Au nanoparticles with diameter of 105 nm ± 13 nm (NanoComposix, Inc.) were first redispersed from H₂O into isopropyl alcohol. Later, AuNPs were sonicated for 20 min., then deposited onto the conjugated polymer spacer by spin-coating a 20 µL drop at a spin rate of 2000 rpm for 40 s. The AuNPs had a poly(vinylpyrrolidone) (PVP) coating of approximately 1 nm to 2 nm. After drying for 2 h in ambient conditions, the sample was ready for characterization.

Reflection-Mode DF Imaging and Correlated AFM Measurements: Heights of AuNPs and surface topography were evaluated using AFM (Nanoscope III, tapping mode, antimony-doped silicon AFM probe tips) and were correlated with true-color,

reflection-mode DF optical images of optical scattering from the AuNPs. True-color, reflection-mode, DF optical images were acquired of regions from each sample prior to AuNP height measurements using a Nikon Optiphot 66 optical microscope equipped with a color CCD camera. A 75 W Xenon lamp was used as the illumination source and DF optical images were both illuminated and collected using a 40X DF objective (numerical aperture (NA) was 0.65). The same regions of the samples were then imaged by AFM. Typically, a region of 20 μm by 20 μm was scanned by AFM at a rate of 5 $\mu\text{m}/\text{s}$. Analysis of the resulting 2D topography profiles was conducted using Gwyddion software. To determine the height of a AuNP, a straight line was drawn across the center of the AuNP under study in the 2D topography profile, which provided the values of “maximum peak height” and “maximum valley depth,” as defined in the software. The height of the AuNP was extracted by adding those two values.

Polarization-Resolved Defocused Dark-Field Imaging: In addition to true-color, reflection-mode DF imaging described above, polarization-resolved, defocused DF imaging of AuNPs was carried out using an inverted microscope (Olympus, IX71) equipped with a variable-NA oil-immersion objective (Olympus, 100X, NA of 0.6 to 1.3). A white-light supercontinuum laser (Fianium WhiteLase WL-SC-400-4) was used for DF illumination of the sample. A half-wave optical retarder was introduced in the laser illumination path to allow the polarization of the laser to be rotated. The incident angle of

the laser on the sample was set to 88° with respect to the surface normal direction to create near-grazing-incidence illumination for DF imaging and so that the polarization of the laser light that illuminated the AuNPs could be controlled (see Figure 5a). Defocused DF optical images were acquired by moving the sample stage $\sim 1 \mu\text{m}$ towards the objective (i.e., along the Z-axis direction) after a focused diffraction-limited DF scattering image was obtained. The defocused scattering signal from the sample was collected by the oil-immersion objective and detected using a single-photon-sensitive, electron-multiplying, charge-coupled device (EMCCD) camera (Andor Technology, iXon), yielding grayscale intensity images of the defocused scattering.

Experimental Dark-Field Back-Scattering Spectra: Experimental DF back-scattering spectra of the SOP systems were collected using a ZEISS AxioVert.A1 inverted microscope operating in a reflection-mode DF configuration, with a broad-spectrum LED light source. Spectra were collected by an Andor Shamrock SR-303i-A imaging spectrometer using an exposure time of 2 s with 15 accumulations and full-vertical-binning mode. In this way each spectrum that was collected sampled an area of that was tens of square micrometers in size; hence, for the SOP samples, multiple AuNPs were probed at once. This gave a scattering spectrum that was an ensemble average of the scattering from between approximately 5 and 50 AuNPs. Ensemble-averaged scattering spectra were obtained from ten different regions of each

SOP sample. The resulting spectra were then post processed in the following manner to obtain ensemble scattering enhancement spectra for the SOP samples relative to a corresponding sample without the AuNPs. First, the background spectrum was subtracted (spectrum of the room, blocking the light source) from each ensemble-averaged scattering spectrum. Next, all of the spectra from the different regions of each sample were averaged. Then the averaged spectrum was divided by the averaged scattering spectrum of corresponding samples without the AuNPs. Finally, the spectra were intensity normalized in order to easily compare the scattering spectral shapes from the different samples (see Figure 2a).

Simulated Dark-Field Back-Scattering Spectra: Commercially-available simulation software based on the finite-difference time-domain method (FDTD Solutions, Lumerical Inc.) was used for electromagnetic simulations of the SOP systems. The refractive index of the environment was set to 1 to mimic air. A broadband, total-field scattered-field (TFSF) source was used to excite the system (propagating at an angle of 10° off the film surface normal) and back-scattering spectra were monitored outside of the TFSF region in order to eliminate contributions from specular reflections. PML boundaries were applied in all x, y and z directions to eliminate effects caused by periodicity of AuNPs.

Conflicts of Interest

There are no conflicts to declare.

Acknowledgements

B. Yu and D. M. O'Carroll acknowledge financial support from National Science Foundation Grant CHE-1415881 (International Collaboration in Chemistry (ICC) Program). M. Vacha acknowledges financial support from JSPS KAKENHI Grant Number JP16107014. J. T. and D. M. O'Carroll acknowledge financial support from National Science Foundation Grant DMR-1554954. The authors gratefully acknowledge helpful discussions with Prof. Piotr Piotrowiak, Prof. Laura Fabris and Prof. Tomokazu Iyoda, and assistance from members of both the O'Carroll and Vacha research groups.

References

1. Nordlander, P. & Le, F. Plasmonic structure and electromagnetic field enhancements in the metallic nanoparticle-film system. *Applied Physics B* 84, 35-41 (2006).
2. Yamamoto, N., Ohtani, S. & García de Abajo, F. J. Gap and Mie plasmons in individual silver nanospheres near a silver surface. *Nano Letters* 11, 91-95 (2010).
3. Chen, X. *et al.* Probing plasmonic gap resonances between gold nanorods and a metallic surface. *The Journal of Physical Chemistry C* 119, 18627-18634 (2015).
4. Li, G.-C., Zhang, Y.-L., Jiang, J., Luo, Y., & Lei, D. Y. Metal-Substrate-Mediated Plasmon Hybridization in a Nanoparticle Dimer for Photoluminescence Line-Width Shrinking and Intensity Enhancement. *ACS Nano* 11, 3067-3090 (2017).
5. Chikkaraddy, R., de Nijs, B., Benz, F., Barrow, S. J., Scherman, O. A., Rosta, E., Demetriadou, A., Fox, P., Hess, O., Baumberg, J. Single-molecule strong coupling at room temperature in plasmonic nanocavities. *Nature* 535, 127-130 (2016).
6. Wind, M., Vlieger, J. & Bedeaux, D. The polarizability of a truncated sphere on a substrate I. *Physica A: Statistical Mechanics and its Applications* 141, 33-57 (1987).
7. Wind, M., Bobbert, P., Vlieger, J. & Bedeaux, D. The polarizability of a truncated sphere on a substrate II. *Physica A: Statistical Mechanics and its Applications* 143, 164-182 (1987).
8. Ruppin, R. Optical absorption by a small sphere above a substrate with inclusion of nonlocal effects. *Physical Review B* 45, 11209 (1992).
9. Prodan, E., Radloff, C., Halas, N. J. & Nordlander, P. A hybridization model for the plasmon response of complex nanostructures. *Science* 302, 419-422 (2003).
10. Aubry, A., Lei, D. Y., Maier, S. A., & Pendry, J. B. Plasmonic hybridization between nanowires and a metallic surface: A transformation optics approach. *ACS Nano* 5, 3293-3308 (2011).
11. Mock, J. J., Hill, R. T., Degiron, A., Zauscher, S., Chilkoti, A. & Smith, D. R. Distance-dependent plasmon resonant coupling between a gold nanoparticle and gold film. *Nano Letters* 8, 2245-2252 (2008).
12. Hill, R. T., Mock, J. J., Urzhumov, Y., Sebba, D. S., Oldenburg, S. J., Chen, S.-Y., Lazarides, A. A., Chilkoti, A., Smith, D. R. Leveraging nanoscale plasmonic modes to achieve reproducible enhancement of light. *Nano Letters* 10, 4150-4154 (2010).
13. Hu, M., Ghoshal, A., Marquez, M. & Kik, P. G. Single Particle Spectroscopy Study of Metal-Film-Induced Tuning of Silver Nanoparticle Plasmon Resonances. *The Journal of Physical Chemistry C* 114, 7509-7514 (2010).
14. Lumdee, C., Toroghi, S. & Kik, P. G. Post-fabrication voltage controlled resonance tuning of nanoscale plasmonic antennas. *ACS Nano* 6, 6301-6307 (2012).
15. Chen, S.-Y. Mock, J. J., Hill, R. T., Chilkoti, A., Smith, D. R., Lazarides, A. A. Gold Nanoparticles on Polarizable Surfaces as Raman Scattering Antennas. *ACS Nano* 4, 6535-6546 (2010).
16. Chen, H. *et al.* Observation of the Fano resonance in gold nanorods supported on

- high-dielectric-constant substrates. *ACS Nano* 5, 6754-6763 (2011).
17. Ha, J. W., Marchuk, K. & Fang, N. Focused orientation and position imaging (fopi) of single anisotropic plasmonic nanoparticles by total internal reflection scattering microscopy. *Nano Letters* 12, 4282-4288 (2012).
 18. Chen, H. *et al.* Effect of the dielectric properties of substrates on the scattering patterns of gold nanorods. *ACS Nano* 5, 4865-4877 (2011).
 19. Li, G.-C., Zhang, Y.-L. & Lei, D. Y. Hybrid plasmonic gap modes in metal film-coupled dimers and their physical origins revealed by polarization resolved dark field spectroscopy. *Nanoscale* 8, 7119-7126 (2016).
 20. Papanikolaou, N. Optical properties of metallic nanoparticle arrays on a thin metallic film. *Physical Review B* 75, 235426 (2007).
 21. G. M. Akselrod, C. Argyropoulos, T. B. Hoang, C. Ciraci, C. Fang, J. Huang, D. R. Smith, M. H. Mikkelsen, Probing the mechanisms of large Purcell enhancement in plasmonic nanoantennas. *Nature Photonics* 8, 835-840 (2014).
 22. D. Y. Lei, A. I. Fernández-Domínguez, Y. Sonnefraud, K. Appavoo, R. F. Haglund Jr., J. B. Pendry, S. A. Maier, Revealing Plasmonic Gap Modes in Particle-on-Film Systems Using Dark-Field Spectroscopy. *ACS Nano* 6, 1380-1386 (2012).
 23. Yu, B., Woo, J., Kong, M. & O'Carroll, D. M. Mode-specific study of nanoparticle-mediated optical interactions in an absorber/metal thin film system. *Nanoscale* 7, 13196-13206 (2015).
 24. Zeng, K., Chen, Z.-K., Shen, L. & Liu, B. Study of mechanical properties of light-emitting polymer films by nano-indentation technique. *Thin Solid Films* 477, 111-118 (2005).
 25. Perevedentsev, A. Chain Conformation and the Photophysics of Polyfluorenes. PhD Thesis, Department of Physics, Imperial College London (2015).
 26. Wang, X.-S. & Feng, X.-Q. Effects of thickness on mechanical properties of conducting polythiophene films. *Journal of Materials Science Letters* 21, 715-717 (2002).
 27. Hahm, S.-W., Hwang, H.-S., Kim, D. & Khang, D.-Y. Buckling-based measurements of mechanical moduli of thin films. *Electronic Materials Letters* 5, 157-168 (2009).
 28. Wang, X.-S., Tang, H.-P., Li X.-D., & Hua X. Investigations on the Mechanical Properties of Conducting Polymer Coating-Substrate Structures and Their Influencing Factors. *International Journal of Molecular Sciences* 10, 5257-5284 (2009).
 29. O'Connor, B., Chan, E. P., Chan, C., Conrad, B. R., Richter, L. J., Kline, R. J., Heeney, M., McCulloch, I., Soles, C. L., DeLongchamp, D. M. Correlations between Mechanical and Electrical Properties of Polythiophenes. *ACS Nano* 4, 7538-7544 (2010).
 30. Savagatrup, S., Makaram, A. S., Burke, D. J. & Lipomi, D. J. Mechanical Properties of Conjugated Polymers and Polymer-Fullerene Composites as a Function of Molecular Structure. *Advanced Functional Materials* 24, 1169-1181 (2014).
 31. Lumdee, C., Yun, B. & Kik, P. G. Effect of surface roughness on substrate-tuned gold

- nanoparticle gap plasmon resonances. *Nanoscale* 7, 4250-4255 (2015).
32. Nanocomposix, Inc., Certificate of Analysis for NanoXact™ (accessed March 20th, 2018).
 33. Haes, A. J., Zou, S., Schatz, G. C. & Van Duyne, R. P. A nanoscale optical biosensor: the long range distance dependence of the localized surface plasmon resonance of noble metal nanoparticles. *The Journal of Physical Chemistry B* 108, 109-116 (2004).
 34. Raether, H. *Surface Plasmons on Smooth and Rough Surfaces and on Gratings*. (Springer-Verlag Berlin Heidelberg 1988).
 35. Böhmer, M. & Enderlein, J. Orientation imaging of single molecules by wide-field epifluorescence microscopy. *J. Opt. Soc. Am. B* 20, 554-559 (2003).
 36. Dedecker, P., Muls, B., Deres, A., Ujiqi, H., Hotta, J., Sliwa, M., Soumillion, J., Müllen, K., Enderlein, J. & Hofkens, J. Defocused Wide-field Imaging Unravels Structural and Temporal Heterogeneity in Complex Systems. *Advanced Materials* 21, 1079-1090 (2009).
 37. Xiao, L., Qiao, Y., He, Y. & Yeung, E. S. Three dimensional orientational imaging of nanoparticles with darkfield microscopy. *Analytical Chemistry* 82, 5268-5274 (2010).
 38. Li, T. *et al.* Three-dimensional orientation sensors by defocused imaging of gold nanorods through an ordinary wide-field microscope. *ACS Nano* 6, 1268-1277 (2012).

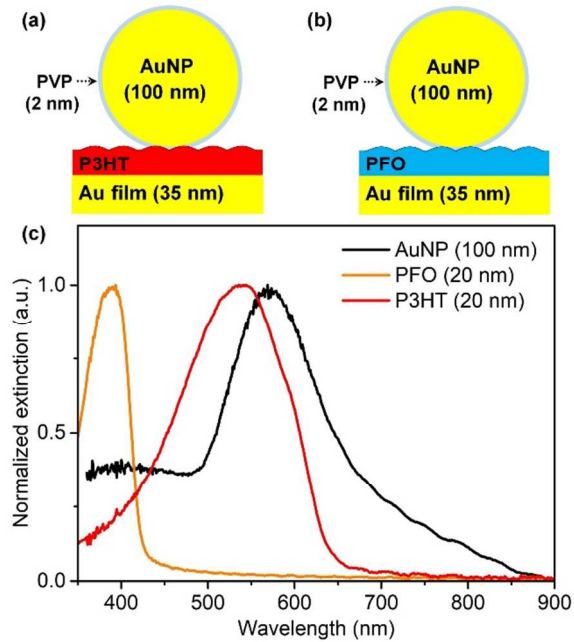


Figure 1. (a,b) Schematics of (a) a AuNP/P3HT/Au film SOP system and (b) a AuNP/PFO/Au film SOP system. (c) Intensity-normalized extinction spectra of 20 nm-thick P3HT and PFO thin films on glass and of 100 nm-diameter AuNPs dispersed in water.

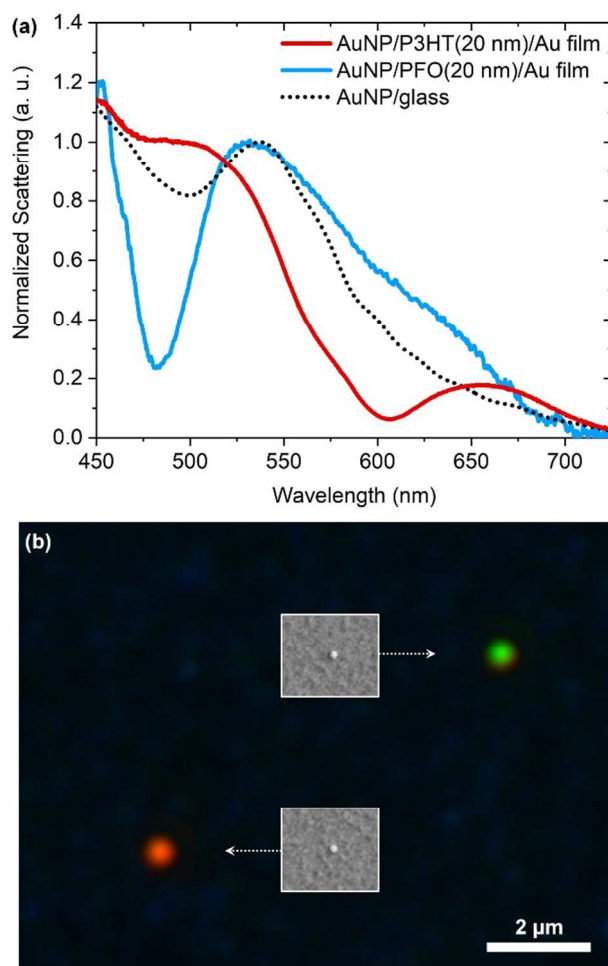


Figure 2. (a) Normalized scattering enhancement spectra of ensembles of AuNP/conjugated polymer/Au film SOP systems relative to conjugated polymer/Au films (red and blue solid curves). The normalized scattering spectrum of an AuNP on glass is shown for comparison (black dotted curve). (b) Dark-field (DF) backscattered light image of AuNP/P3HT/Au film sample showing two AuNPs with different scattering colors. The P3HT film is 50 nm thick. Insets: Scanning electron microscope images of the same two AuNPs shown in the main DF image.

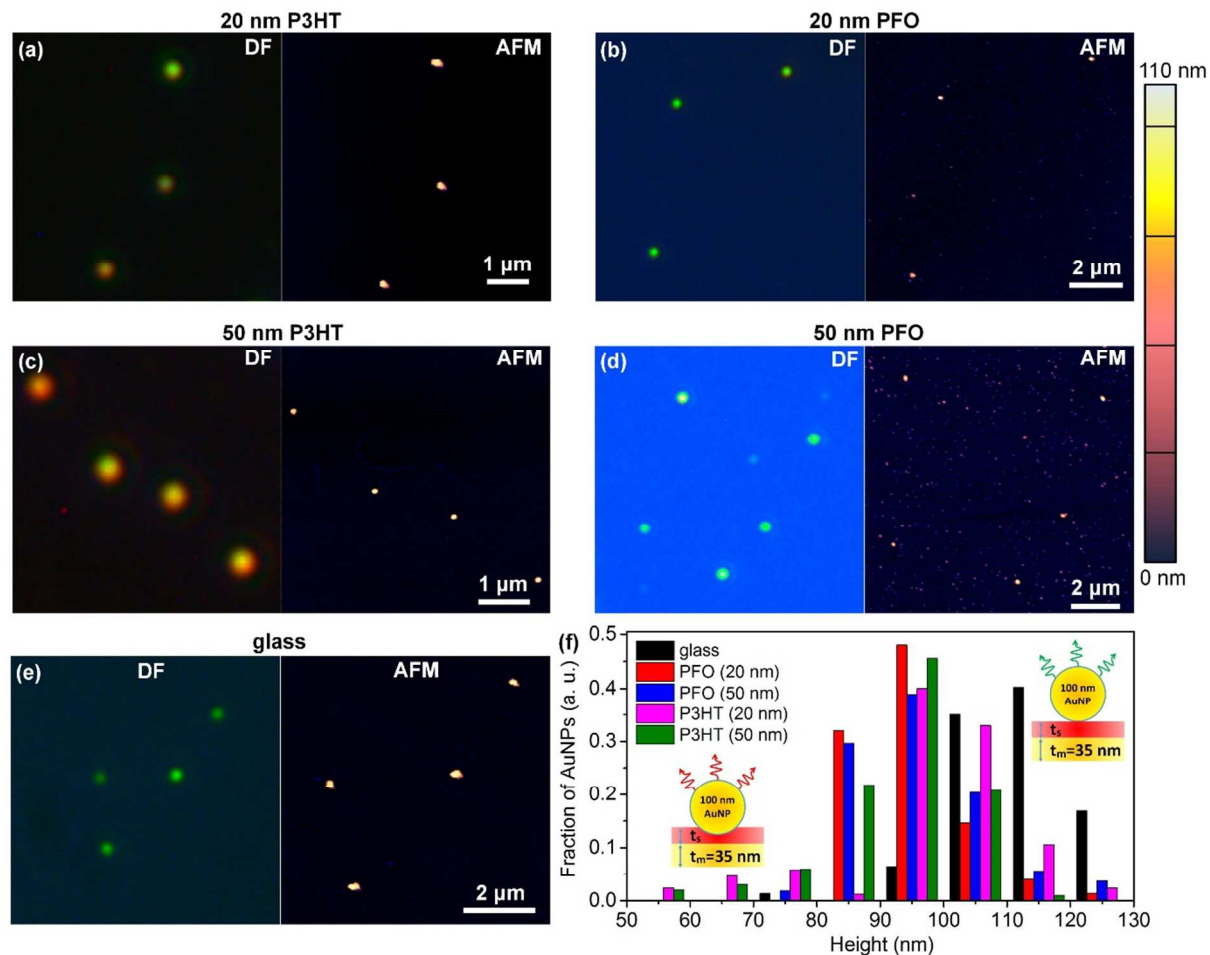


Figure 3. DF optical images showing back-scattered light, and 2D AFM topography profiles of corresponding sample areas with 100-nm-diameter AuNPs on: (a) a 20-nm-thick P3HT spacer film; (b) a 20-nm-thick PFO spacer film; (c) a 50-nm-thick P3HT spacer film; (d) a 50-nm-thick PFO spacer film; and (e) a glass substrate. All P3HT and PFO films in (a)-(d) were on a 35-nm-thick Au film on a glass substrate. The height scale bar for all of the 2D AFM topography profiles is shown on the right of (b) and (d). (f) Histogram of AuNP heights on the different underlying media specified for (a) to (e). Insets in (f) depict the difference of back-scattering color of AuNPs with various heights with and without embedding in P3HT.

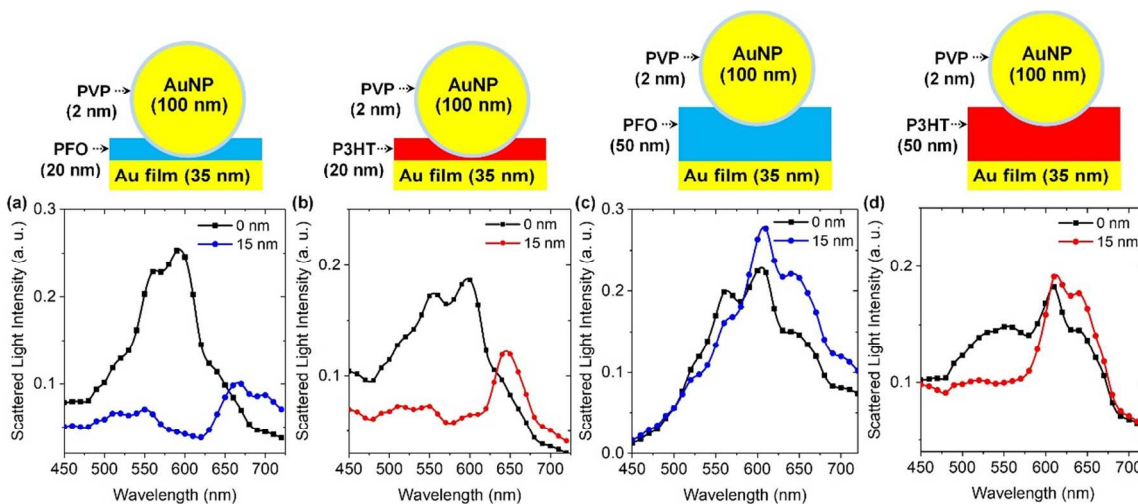


Figure 4. (a-d) Simulated back-scattering spectra of SOP systems (indicated by the corresponding schematics on top) with 15 nm of AuNP embedding in the polymer spacer (colored circles) and without AuNP embedding (black squares). (a) Back-scattering spectra from a single AuNP/PFO/Au film SOP system with a 20 nm-thick PFO spacer. (b) Back-scattering spectra from a single AuNP/P3HT/Au film SOP system with a 20 nm-thick P3HT spacer. (c) Back-scattering spectra from a single AuNP/PFO/Au film SOP system with a 50 nm-thick PFO spacer. (d) Back-scattering spectra from a single AuNP/P3HT/Au film SOP system with a 50 nm-thick P3HT spacer. A 2 nm-thick PVP layer covered the AuNP in all simulations.

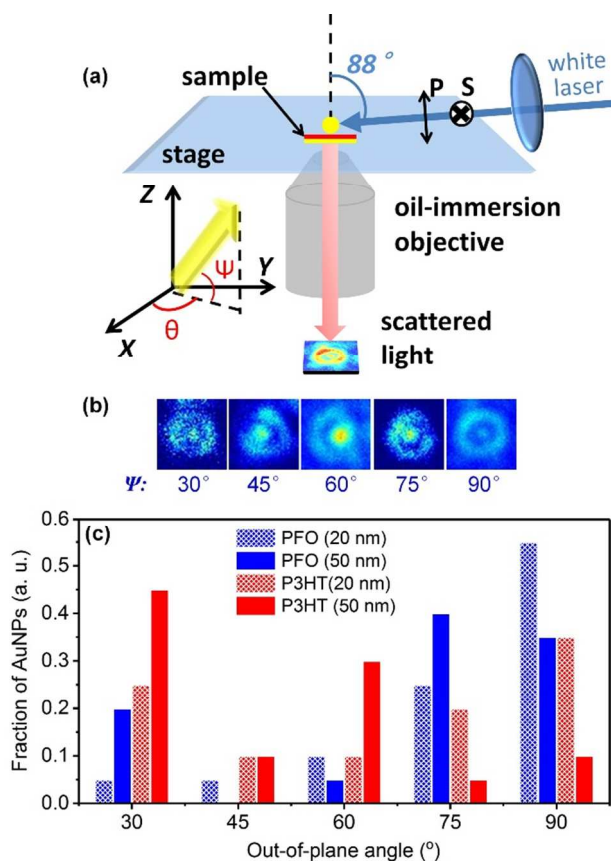
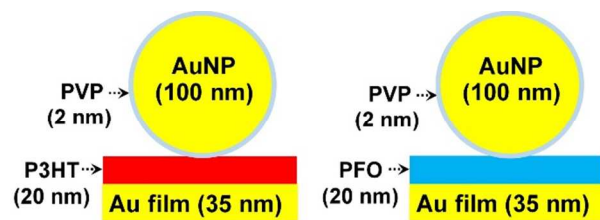


Figure 5. (a) Schematic diagram of the broadband defocused imaging setup. P-polarized illumination was employed to excite the vertical modes primarily. Ψ and θ indicate polar (out-of-plane) and azimuthal (in-plane) angles, respectively. (b) shows the representative defocused images of SOP systems with various Ψ . (c) Distribution of Ψ for AuNP/polymer spacer/Au film SOP systems with various polymer spacers: 20-nm-thick and 50-nm-thick PFO; 20-nm-thick and 50-nm-thick P3HT. The spacers were all sandwiched between AuNPs (~ 100 nm diameter) and a 35-nm-thick Au film.



Scattering color changes are investigated in plasmonic sphere-on-plane samples containing resonant and non-resonant conjugated polymer spacers.